第31卷 第2期 焊 接 学 报 Vol. 31 No. 2
2010年2月 TRANSACTIONS OF THE CHINA WELDING INSTITUTION February 2010

激光再制造金属零件熔覆层组织及耐磨性能

张晓东[1,2]， 董世运[2]， 王志坚[2]， 闫世兴[2]， 徐滨士[2]， 李庆芬[1]

（1. 哈尔滨工程大学 材料科学与化学工程学院，哈尔滨 150001；
2. 装甲兵工程学院 装备再制造技术国防科技重点实验室，北京 100072）

张晓东

摘 要：采用 Fe-Cr-B-Si-Mo 铁基合金粉末进行激光多层熔覆，利用金相显微镜（OM），扫描电镜（SEM），显微硬度计和磨损试验机分析了熔覆层的显微组织，测试了涂层的硬度和耐磨性能. 试验发现，多层熔覆层组织致密，具有快速凝固组织特征；层间形成了冶金结合，从而使整个材料在理论上没有薄弱环节. 结果表明，熔覆层硬度达到 760～780 HV；45 钢基体的体积磨损量是激光熔覆层的 21.7 倍；激光熔覆层具具有较好的冶金质量和耐磨性.

关键词：激光再制造；组织；耐磨性能

中图分类号：TG115.28 **文献标识码**：A **文章编号**：0253－360X(2010)02－0075－04

0 序 言

再制造是废旧机电产品高技术修复与改造的产业化. 它以产品全寿命周期理论为指导，以优质、高效、节能、节材、环保为准则，以先进技术和产业化生产为手段，再制造产品的质量和性能要达到或超过新品[1]. 目前，再制造已得到中国政府、学术界和企业界的广泛认同与支持，是发展循环经济、构建节约型社会的重要组成部分. 改革开放以来，国外大批的高精尖设备引入中国，许多重大工程装备造价十分昂贵，一旦出现损坏，使生产线中断. 特别是进口设备，缺少备件，临时引进不仅价格昂贵，而且时间紧迫，不能保证及时生产，将造成重大的经济损失. 因此，开展重大装备修复，发展快速、高效、精密的修复技术不仅具有广阔的市场需求，而且具有重大的经济效益和社会效益[2]. 激光再制造技术，不仅能够使损坏的零件恢复原有或近似原有尺寸，而且可以提高性能，节约费用，为再制造金属零件提供了可行的先进制造技术[3－5]. 激光熔覆硬面耐磨涂层应用于表面改性和表面修复领域已经很多年，其中铁基合金具有价格便宜，工艺性好等特点，适用于激光熔覆恢复工件尺寸，在磨损零件修复中具有较大优势. 在实际应用中，需要多层堆积才能够满足磨损零件尺寸恢复的要求，多层堆积组织特点和性能已经引起国内外学者的广泛重视[6－8]，但对 Fe-Cr-B-Si-Mo 铁基合金多层堆积熔覆层组织和性能研究较少. 为此，采用连续波 Nd∶YAG 固体激光器在 45 钢表面激光熔覆多层堆积 Fe-Cr-B-Si-Mo 铁基合金粉末，并对多层堆积熔覆层的组织特点、硬度分布及耐磨性能进行了研究，为激光再制造耐磨零件提供参考.

收稿日期：2009－08－20
基金项目：国家自然科学基金重点资助项目（50735006）；国家 973 计划资助项目（2007CB607601）

1 试验方法

试验用基体材料为 45 钢，试样尺寸为 100 mm×10 mm×80 mm. 先用 600 目砂纸打磨试样，然后用丙酮清洗，最后在空气中烘干. 激光熔覆材料选用 Fe-Cr-B-Si-Mo 铁基合金粉末，粉末粒度为－140～325 目，其化学成分（质量分数，%）为 Cr13.5，B1.65，Si1.15，Mo0.8，Fe 余量. 试验前，对粉末进行真空烘干处理，以去除粉末表面吸附的水分.

采用 1 kW 连续波 Nd∶YAG 固体激光器进行激光熔覆，激光束波长为 1.06 μm，光斑直径为 2 mm，在机器人控制下实现激光再制造，金属粉末通过侧向送粉方式送入激光熔池. 优化的激光处理工艺参数为功率 1 kW，扫描速度 5 mm/s，送粉量 3.0 g/min，Z 轴抬升量 0.25 mm，搭接率 40%；采用氩气保护激光熔池.

采用光学显微镜（OM）分析了试样的显微组织. 利用 HVS—1000 型显微硬度计测量熔覆层横截面的硬度，硬度计载荷 1.96 N，持载时间 15 s. 摩

擦磨损试验在 UMT—2 型多功能摩擦磨损试验机上进行,摩擦对偶球为 Φ 4 mm 的 GCr15 钢球,其硬度为 65 HRC. 摩擦试验条件和参数为:在干摩擦条件下往复滑动,行程为 4.7 mm,频率为 5 Hz,载荷为 30 N,摩擦时间为 20 min. 通过测量磨痕宽度,利用文献[9]方法计算磨损体积损失,评价材料的耐磨性. 对磨痕宽度 d 进行测量,最终结果取 5 次试验的平均值,磨损量体积为

$$\nabla V = L\left[R^2 \arcsin\left(\frac{d}{2R}\right) - \frac{1}{2}d\sqrt{R^2 - \frac{1}{4}d^2}\right] \quad (1)$$

式中:R 为钢球半径;d 为磨痕宽度;L 为往复滑动行程;ΔV 为磨损体积.

2 试验结果与分析

2.1 熔覆层显微组织分析

图 1 是单道多层堆积试样横截面金相组织. 从图 1a 中可以看出:熔覆层与基体之间无裂纹、气孔等缺陷,界面处出现了大约 20 μm 厚的“白亮带”,它是以平面晶的生长形态沿热流方向生长出来的. 这是由于凝固过程中,熔池底部凝固速度趋近于 0,所以出现了平界面的生长形态;“白亮带”的形成使得基体和涂层之间形成良好的冶金结合. 而在涂层内部则为细小的定向凝固柱状枝晶,如图 1b,由于铁基合金是面心立方结构,在正温度梯度下,与热流方向最为接近的 <100> 择优取向优先生长,并在后续沉积的过程中不断的外延生长,将在整个涂层中得到完全的细小定向凝固柱状枝晶. 这种超细的定向凝固组织是由于激光熔池中的极高的温度梯度和大的冷却速率决定的. 从图 1c 可以看出:成形层层间以冶金结合的方式结合在一起的,这不仅保证了层间的结合强度,还保证了外延组织在生长方向上的连续性,因此可以消除低强度界面对材料性能的不利影响. 另外,由图 1c 还可发现多层熔覆层中前一层的组织发生了粗化,这是由于多层堆积过程中,导致已经凝固的任何一点处,都经受反复加热、冷却的再热循环过程. Griffith 等人[10]的研究表明,对已经熔覆的某一点而言,当熔池位于其正上方时,在正在进行加工的熔覆层上,热源距离该点处的距离最近,因而该点处出现温度的蜂值;当熔池不在正上方时,该点的温度逐渐下降到最低. 随着熔覆过程的不断进行,该点处温度呈震荡衰减变化.

对于先前形成的组织,经历了足够多次较高温度的再热循环后,相当于进行了一段时间的时效、退火处理,进而发生组织的粗化. 图 1d 为多层堆积熔覆层的顶部显微组织,从图1d中可以看出:熔覆层

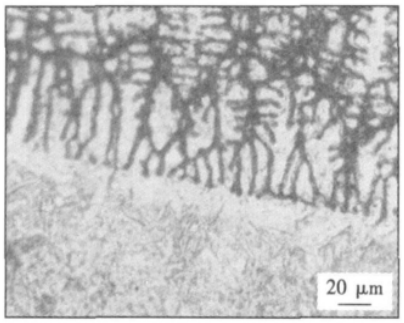

(a) 界面组织

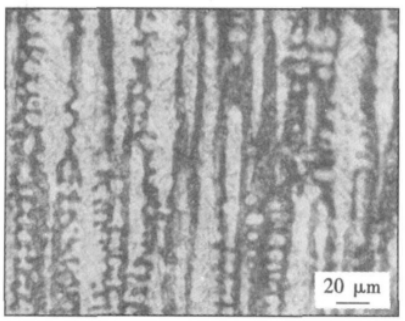

(b) 层内组织

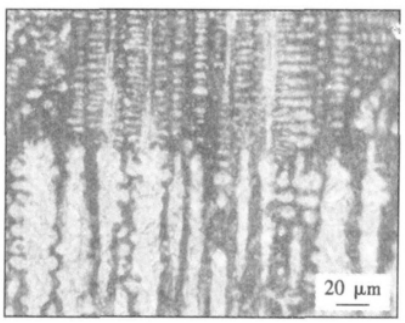

(c) 层间组织

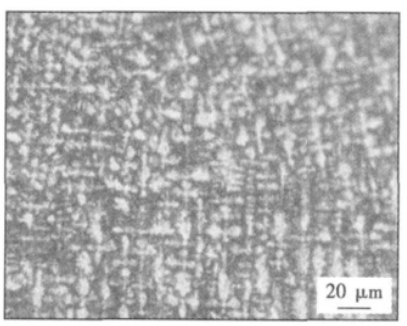

(d) 顶部组织

图 1 单道多层堆积试样横截面金相组织形貌

Fig. 1 Microstructure of transverse section of single path multi-layer sample

顶部组织与层内和底部组织不同,顶部出现细小的等轴晶. 这是由于在熔池顶部,温度梯度 G 减小,凝固速度 v 增大,G/v 比值减小,“成分过冷”增大,且在熔池顶部通过与气氛对流、辐射等方式冷却,前一层的部分晶粒重熔,形成新的晶核,落入熔池顶部未熔化的金属粉末也成为新的形核核心,故在熔池顶

部可形成一层等轴晶,在试样中部没有出现此种等轴晶组织是因为在逐层熔化沉积过程中熔池顶部组织已被逐层重熔掉.

2.2　熔覆层的显微硬度

图 2 为单道多层堆积试样沿纵向的硬度分布曲线,从图中可以看出:硬度分为三个区域,分别对应基体、过渡区和涂层区. 过渡区硬度随着深度的增加而逐渐下降. 涂层的硬度范围为 760 ~ 780 HV 之间. 熔覆层的硬度远高于基体,高的硬度为熔覆层具有较好的耐磨性提供了保证.

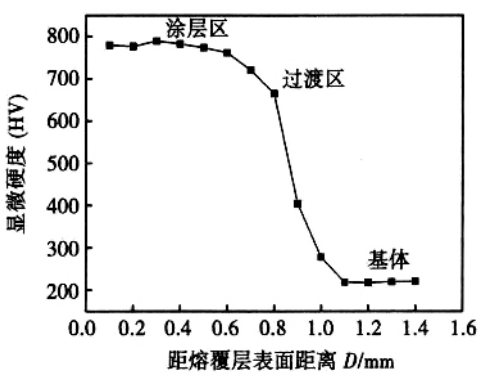

图 2　单道多层堆积试样的显微硬度分布曲线

Fig. 2　Hardness distribution curve of single path multi-layer sample

2.3　熔覆层的耐磨性能

图 3 显示了 45 钢基体和激光熔覆层在干摩擦条件下的磨损性能. 由图 3 可知:45 钢基体的体积磨损损失量大约是激光熔覆层的 21.7 倍. 图 4 为激光熔覆层和 45 钢摩擦系数随时间的变化曲线,可以看出:激光熔覆层的摩擦系数小于 45 钢的摩擦系数. 图 5 为 45 钢基体和激光熔覆层磨痕形貌,45 钢基体的犁沟较深且有塑性变形,粘着现象较严重,是典型的粘着磨损和磨料磨损特征;而激光熔覆层的磨痕较浅,其上有磨屑脱落痕迹,是典型的磨料磨损特征. 在法向载荷作用下,硬质 GCr15 磨球上与材料表面接触的微观凸出部分嵌入材料表面,在滑动过程中推挤并切削硬度相对较低的材料,使韧性好的材料发生塑性变形并导致疲劳破坏,使脆性材料破碎并脱落. 在激光熔覆层较高的硬度(45 钢的硬度为 230 HV,熔覆层的硬度为 760 ~ 780 HV),是其耐磨性能得以提高的主要原因.

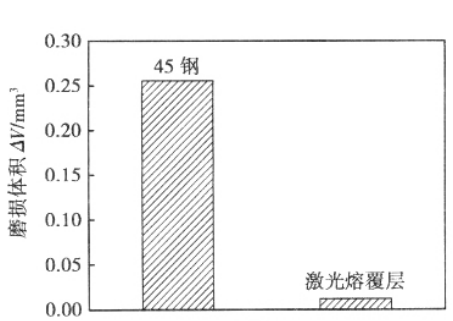

图 3　激光熔覆层和 45 钢磨损性能

Fig. 3　Wear resistance property of laser clad and 45 steel

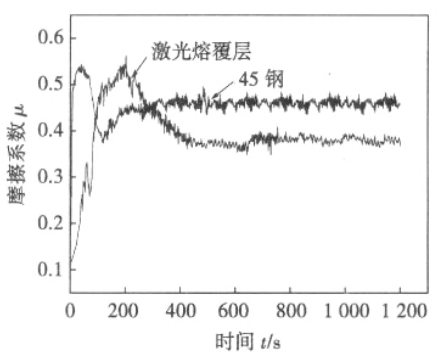

图 4　摩擦系数随时间变化曲线

Fig. 4　Curves of friction coefficient vs time during wear test

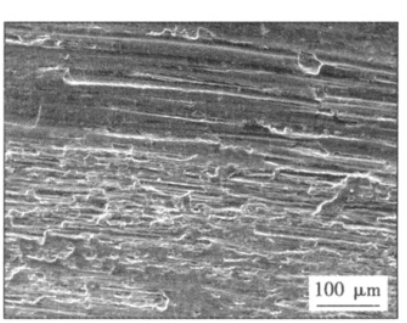

(a) 45 钢

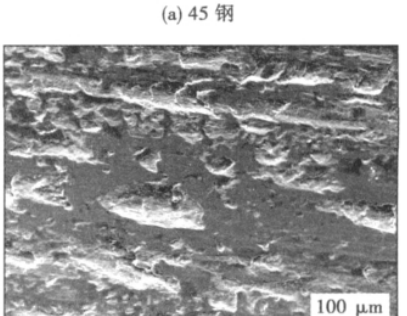

(b) 激光熔覆层

图 5　磨损试样表面 SEM 形貌

Fig. 5　Worn surface morphologies of sample

4　结　　论

(1) 在 45 钢金属表面激光熔覆制备了 Fe-Cr-B-Si-Mo 多层堆积熔覆层,熔覆层组织致密,具有快

速凝固组织特征,层间组织实现了冶金结合. 但是,多层熔覆沉积使得先期沉积熔覆层组织发生一定程度的粗化现象.

(2) 激光熔覆 Fe-Cr-B-Si-Mo 熔覆层硬度达到 760 ~ 780HV,具有良好耐磨性,其相对耐磨性是 45 钢基体的 21.7 倍.

参考文献:

[1] 徐滨士. 装备再制造工程的理论与技术[M]. 北京:国防工业出版社, 2007.

[2] 杨洗陈, 李会山, 刘运武, 等. 激光再制造技术及其工业应用[J]. 中国表面工程, 2003, 4:43 - 46.
Yang Xichen, Li Huishan, Liu Yunwu, *et al*. Laser remanufacturing technology and its industrial application[J]. China Surface Engineering, 2003, 4:43 - 46.

[3] 李会山, 杨洗陈, 王云山, 等. 激光再制造过程熔池温度场的数值模拟[J]. 天津工业大学学报, 2003, 22(5):9 - 12.
Li Huishan, Yang Xichen, Wang Yunshan, *et al*. Numerical simulation for temperature field in molten pool of laser remanufacturing processing[J]. Journal of Tianjin Polytechnic University, 2003, 22(5):9 - 12.

[4] Dong Shiyun, Xu Binshi, Wang Zhijian, *et al*. Laser remanufacturing technology and its applications[J]. Proceedings of SPIE, 2007, 6825:68251N - 1 - 68251N - 5

[5] Song Jianli, Deng Qinlin, Chen Changyuan, *et al*. Rebuilding of metal components with laser cladding forming[J]. Applied Surface Science, 2006, 252:7934 - 7940.

[6] Majumdar J D, Pinkerton A, Liu Z, *et al*. Microstructure characterization and process optimization of laser assisted rapid fabrication of 316L stainless steel[J]. Applied Surface Science, 2005, 247:320 - 327.

[7] Zhao Xiaoming, Chen Jing, Lin Xin. Study on microstructure and mechanical properties of laser rapid forming inconel 718[J]. Materials Science and Engineering A, 2008, 478:119 - 124.

[8] Qu H P, Wang H M. Microstructure and mechanical properties of laser melting deposited γ-TiAl inter-metallic alloys[J]. Materials Science and Engineering A, 2007, 466:187 - 194.

[9] Shen Longguang, Zhang Qingmao, Song Jie, *et al*. Investigation on tribological behavior of Fe-based alloy coating formed by laser cladding[J]. Lasers in Material Processing and Manufacturing Ⅲ, 2007, 6825:68251P - 1 - 68251P - 3.

[10] Griffith M L, Schlienger M E, Harwell L D, *et al*. Understanding thermal behavior in the LENS process[J]. Materials and Design, 1999, 20:107 - 113.

作者简介:张晓东,男,1981 年出生,博士研究生. 主要从事再制造工程方面的研究. 发表论文 4 篇.

Email:syd422@ vip. sohu. com

[上接第 66 页]

[3] 王希靖, 韩晓辉, 郭瑞杰, 等. 搅拌摩擦焊接过程温度场数值模拟[J]. 焊接学报, 2005, 26(12):18 - 20.
Wang Xijing, Han Xiaohui, Guo Ruijie, *et al*. Numerical simulation of temperature field in friction stir welding[J]. Transactions of the China Welding Institution, 2005, 26(12):18 - 20.

[4] 胡礼木, 胡 波. 搅拌摩擦焊焊接温度场数值模型及其影响因素[J]. 机械工程学报, 2007, 42(7):235 - 238.
Hu Limu, Hu Bo. Numeric model of welding temperature in friction stir welding and affecting factors[J]. Chinese Journal of Mechanical Engineering, 2007, 42(7):235 - 238.

[5] Frigaard O. A process model for friction stir welding of age hardening aluminum alloy[J]. Metallurgical and Materials Transactions, 2001, 32(5):1189 - 1200.

作者简介:徐韦锋,男,1982 年出生,博士研究生. 主要研究厚板铝合金搅拌摩擦焊接、模拟和腐蚀性能. 已发表论文 8 篇.

Email:xwf1982@ mail. nwpu. edu. cn

of laser keyhole welding process is considered with the model based on the multiple reflections Fresnel absorptions, the jump boundary conditions of the keyhole wall, the radiation heat transfer of vapor plume/plasma, the Marangoni force, the friction force in the solid-liquid mixture phase, the buoyancy force, the viscous force, the evaporation latent and the solidification/melting latent, and the conduction, convection and radiation heat transfer of the metal alloys. A Level Set method and a new Fast Sweeping method are developed to solve the transient keyhole evolution equations. A SOLA method is proposed to solve the three-dimensional heat transfer and fluid flow of the transient weld pool. Numerical examples demonstrate that the presented model can be used to reasonably simulate the transient keyhole behaviors and the transient weld pool dynamics during laser keyhole welding.

Key words: laser keyhole welding; mathematical model; transient keyhole; transient weld pool

Microstructure and wear resistance of clad layer on laser remanufacturing metal pieces ZHANG Xiaodong[1,2], DONG Shiyun[2], WANG Zhijian[2], YAN Shixing[2], XU Binshi[2], Li Qingfen[1] (1. School of Material Science and Chemical Engineering, Harbin Engineering University, Haerbin 150001, China; 2. National Key Laboratory for Remanufacturing, Academy of Armored Force Engineering, Beijing 100072, China). p 75 - 78

Abstract: The microstructure, hardness, wear resistance of cladding layer, which Fe-Cr-B-Si-Mo alloy powders were clad by using laser multi-layer on the 1045 steel substrate, were researched with scanning electron microscope, optical microscopy, micro-hardness tester and wear testing machine. The results show that the microstructure of the layer is fully dense with rapidly solidified microstructure. There is a metallurgical bonding between layer and layer, so no weakness in the whole material in theory. The hardness of the laser is about 760-780 HV. The wear resistance of laser cladding coatings is 21.7 times higher than that of the unclad 45 steel. Laser cladding layer has higher metallurgy quality and wear resistance.

Key words: laser remanufacturing; microstructure; wear resistance behavior

Investigation and application of ultrasonic-TIG hybrid welding equipment SUN Qingjie, LIN Sanbao, YANG Chunli, YAN Jiuchun (State Key Laboratory of Advanced Welding Production Technology, Harbin Institute of Technology, Harbin 150001, China). p 79 - 82

Abstract: The limitations of the TIG welding include low productivity due to low deposition rates, shallow penetration, and inconsistent penetration in the stainless steel plate with 5 mm thickness. An ultrasonic assisted TIG welding equipment with the assistance of high-intensity ultrasonic was researched and developed to increase the welding penetration and improve the welding efficiency. The frequency and the output power of the ultrasonic are respectively adjusted by the input voltages of the control circuit and the main circuit. The output power of the ultrasonic vibration can be continuously adjusted from 0 W to 1 000 W. Experimental results show that the high-intensity ultrasonic has the effect of increasing the weld penetration. Also, the process is simple and easy-controlled compared with other welding methods for increasing penetration. The ultrasonic assisted TIG welding equipment can satisfy the requirements of the design and application.

Key words: ultrasonic vibration; resonance; acoustic field; stainless steel; welding penetration

Characteristics of aluminium-lithium alloy joint formed by YAG-MIG hybrid welding YANG Jing[1,2], LI Xiaoyan[1], GONG Shuili[2], CHEN Li[2], XU Fei[1,2] (1. College of Material Science and Engineering, Beijing University of Technology, Beijing 100124, China; 2. Key Laboratory for High Density Beam Processing Technology, Beijing Aeronautical Manufacturing Technology Research Institute, Beijing 100124, China). p 83 - 86

Abstract: The process of YAG laser and MIG-arc hybrid welding for 5A90 aluminium-lithium alloy was investigated based on analysing the characteristics of joint formation in laser-arc hybrid welding. Under the condition of the constant welding position, the effect of main welding parameters on the joint formation, including laser power, travel speed, welding current and the distance between hybrid thermal sources, was discussed. The results indicate that a good synergistic effect is shown if the distance between laser and arc is within 0-6 mm. The laser power plays a main role in increasing of depth and backside width of weld. With the increase of welding speed, the width of the weld decreases rapidly, so dos the penetration. But the depth and width of the weld increase obviously with the promotion of welding current.

Key words: aluminium-lithium alloy; laser-arc hybrid welding; weld formation

Inversion imaging of nugget cross-section in aluminum alloy resistance spot welding XUE Zhiqing[1], LUO Zhen[1], SHAN Ping[1], LIU Ying[2], Wang Rui[1] (1. School of Materials Science and Engineering, Tianjin University, Tianjin 300072, China; 2. Jinghai County's Commission on Science and Technology in Tianjin, Tianjin 301600, China). p 87 - 90

Abstract: Inverse theory and regularization method are used to the current inversion imaging of nugget cross-section. The inversion image can be used to evaluate spot weld intuitively, which meets to the requirements of higher weld quality. Firstly, the forward model which describes the relationship between the current distributions of nugget cross-section and magnetic field was established, and its reliability was verified by experiments. Secondly, the inversion model was established and the numerical experiments were conducted to verify correctness of the inversion model. In the end, different current values were chosen for the resistance spot welding experiments, and then the collected magnetic signals were transformed into current signals, which were displayed in the form of image. Experiment results show that the inversion image can describe the characteristics of nugget cross-section current distribution and reflect the quality of nug-